



ELSEVIER

Available online at www.sciencedirect.com

SCIENCE @ DIRECT®

PHYSICS LETTERS B

Physics Letters B 583 (2004) 59–67

www.elsevier.com/locate/physletb

Antihydrogen production temperature dependence

ATHENA Collaboration

M. Amoretti^a, C. Amsler^b, G. Bazzano^c, G. Bonomi^{d,*}, A. Bouchta^d, P.D. Bowe^e,
C. Canali^{a,f}, C. Carraro^{a,f}, C.L. Cesar^g, M. Charlton^e, M. Doser^d, A. Fontana^{c,h},
M.C. Fujiwara^{i,j}, R. Funakoshi^j, P. Genova^{c,h}, J.S. Hangst^k, R.S. Hayano^j, I. Johnson^b,
L.V. Jørgensen^e, A. Kellerbauer^d, V. Lagomarsino^{a,f}, R. Landua^d, E. Lodi Rizzini^{c,l},
M. Macrì^a, N. Madsen^{b,k}, G. Manuzio^{a,f}, M. Marchesotti^d, D. Mitchard^e, F. Ottone^{c,h},
H. Pruyss^b, C. Regenfus^b, P. Riedler^d, A. Rotondi^{c,h}, G. Testera^a, A. Variola^a,
L. Venturelli^{c,l}, Y. Yamazakiⁱ, D.P. van der Werf^e, N. Zurlo^{c,l}

^a *Istituto Nazionale di Fisica Nucleare, Sezione di Genova, 16146 Genova, Italy*

^b *Physik-Institut, University of Zurich, CH-8057 Zürich, Switzerland*

^c *Istituto Nazionale di Fisica Nucleare, Sezione di Pavia, 27100 Pavia, Italy*

^d *EP Division, CERN, CH-1211 Geneva 23, Switzerland*

^e *Department of Physics, University of Wales Swansea, Swansea SA2 8PP, UK*

^f *Dipartimento di Fisica, Università di Genova, 16146 Genova, Italy*

^g *Instituto de Fisica, Universidade Federal do Rio de Janeiro, Rio de Janeiro 21945-970, Brazil*

^h *Dipartimento di Fisica Nucleare e Teorica, Università di Pavia, 27100 Pavia, Italy*

ⁱ *Atomic Physics Laboratory, RIKEN, Saitama 351-0198, Japan*

^j *Department of Physics, University of Tokyo, Tokyo 113-0033, Japan*

^k *Department of Physics and Astronomy, University of Aarhus, DK-8000 Aarhus C, Denmark*

^l *Dipartimento di Chimica e Fisica per l'Ingegneria e per i Materiali, Università di Brescia, 25123 Brescia, Italy*

Received 19 November 2003; accepted 7 January 2004

Editor: W.-D. Schlatter

Abstract

Cold antihydrogen atoms were produced by mixing cold samples of antiprotons and positrons. The temperature of the positron plasma was increased by controlled radio-frequency (RF) heating, and the antihydrogen production was measured. Formation is observed to decrease with increased temperature but a simple power law scaling is not observed. Significant production is still present at room temperature.

© 2004 Published by Elsevier B.V.

PACS: 36.10.-k; 52.70.-m

Keywords: Antihydrogen; Recombination; Nested trap; Positron plasma; Antiprotons

* Corresponding author.

E-mail address: germano.bonomi@cern.ch (G. Bonomi).

1. Introduction

Cold antihydrogen ($\bar{\text{H}}$) atoms have recently been produced by two experiments at CERN. First ATHENA [1] and then ATRAP [2] reported the creation of samples of cold antihydrogen by mixing antiprotons (\bar{p} 's) and positrons (e^+ 's) at low temperature in a nested Penning trap [3]. Under these conditions the two main processes [4] expected to be important for $\bar{\text{H}}$ formation are radiative combination and three body combination [5–7]. The two mechanisms lead to different quantum state populations of the antiatoms, and have different dependence on the positron plasma density and temperature. Important insights into the formation mechanism and state distribution can therefore be obtained by studying the temperature dependence of the production of antihydrogen. A better knowledge of the state distribution, and how to influence it, is needed in order to prepare states that can be trapped and studied. For instance, precision spectroscopy of antihydrogen promises high precision CPT tests building on accurate hydrogen spectroscopy [8,9]. In this Letter we present the first studies of the temperature dependence of antihydrogen production.

2. Antihydrogen production

2.1. Overview

The ATHENA experiment uses antiprotons delivered by CERN's Antiproton Decelerator (AD) and positrons emitted from a ^{22}Na radioactive source (1.4×10^9 Bq). Both the \bar{p} 's and the e^+ 's are trapped, cooled and accumulated prior to mixing in a nested Penning trap. This trap configuration allows simultaneous trapping of oppositely charged particles. The 3 Tesla solenoidal magnetic field which provides the radial confinement also allows positrons to cool efficiently (with a time constant $\tau \simeq 0.5$ s) to the trap temperature by the emission of synchrotron radiation [10]. The trap is kept at a temperature of ~ 15 K and the mixing region at a pressure of less than 10^{-12} mbar. In a "standard mixing cycle" the central part of the nested trap is filled with about 7×10^7 e^+ 's. Once the positrons have self-cooled, about 10^4 \bar{p} 's are injected at about 30 eV and the two particle species allowed to interact for about 3 minutes. At the end of the mix-

ing cycle the nested trap is emptied and the process restarted.

Neutral $\bar{\text{H}}$ atoms escape the confinement region and annihilate on the trap electrodes producing on average about five pions (charged and neutral) from the \bar{p} annihilation, and two 511 keV γ 's from the e^+ annihilation (the 3γ contribution to our $\bar{\text{H}}$ signal does not exceed 5% [11]). The nested trap is surrounded by a detector that allows reconstruction of $\bar{\text{H}}$ annihilations [12]. Charged particles are detected by two layers of double sided silicon micro-strip detectors. The reconstruction efficiency for \bar{p} annihilation vertices is about 50%. Photons from positron annihilations are detected by CsI crystals with an efficiency of about 20% per photon. Their energy is also measured with a resolution of 24% (FWHM). Detector readout is triggered when at least three sides in the outer silicon modules are hit. Our trigger efficiency for $\bar{p}(\bar{\text{H}})$ annihilations is $85 \pm 10\%$ and this value has been used to correct all the data presented here. The detector intrinsic trigger dead time, in absence of readout, is about 2 μs . At the beginning of readout the detector trigger is masked for 300 μs to avoid digital cross talk. This is therefore our maximum trigger dead time which is negligible given a maximum rate of 400 Hz. However, the complete readout of the detector takes about 10 ms and high event rates may lead to saturation of the readout. This effect was monitored and corrected for. More details about the experimental setup and the data acquisition system can be found elsewhere [13].

2.2. Positron plasma temperature

Synchrotron cooling of positrons and the inter-particle Coulomb collisions are expected, in the absence of externally applied perturbations, to bring the plasma into thermal equilibrium with the surrounding electrodes, which have a temperature of ~ 15 K. In equilibrium the positron plasma rotates semi-rigidly around the magnetic field axis. Theoretical models [10,14,15] and experimental studies [16] indicate that the positron velocity distribution in the rotating reference frame is Maxwellian with a thermal equilibration rate of a few tens of kHz [17]. The antiprotons are cooled by the positrons through Coulomb collisions [18–20] in tens of ms. For heated positrons, the cooling time is somewhat slower (< 1 s). At thermal equi-

Table 1

Summary of the results of measurements with different positron plasma temperatures. ΔT is the temperature increase. “ \bar{p} 's” is the total number of antiprotons used in the mixing cycles. The “ $\cos(\theta_{\gamma\gamma})$ excess” is the opening angle excess and “peak” is the peak trigger rate (see text for details). These quantities are available only for the high statistics samples. The integrated number of triggers for different time intervals from the start of mixing cycle are also reported. All the values were normalized to a standard cycle with $10^4 \bar{p}$'s. The errors in ΔT represent the maximum systematic uncertainty. The errors in $\cos(\theta_{\gamma\gamma})$, peak trigger rate, and number of triggers are each the combination of statistical and systematic errors

ΔT (meV)	\bar{p} 's	$\cos(\theta_{\gamma\gamma})$ excess	Peak (Hz)	Triggers	
				3 s	180 s
0	$(2.94 \pm 0.21) \times 10^6$	1.65 ± 0.19	454 ± 44	441 ± 40	2612 ± 240
3_{-3}^{+15}	$(3.46 \pm 0.25) \times 10^4$	–	–	395 ± 38	2409 ± 222
7_{-7}^{+15}	$(4.08 \pm 0.29) \times 10^4$	–	–	338 ± 32	2233 ± 206
15 ± 15	$(1.82 \pm 0.13) \times 10^6$	1.08 ± 0.15	381 ± 38	352 ± 32	1981 ± 181
25 ± 15	$(3.13 \pm 0.22) \times 10^4$	–	–	214 ± 22	1683 ± 156
43 ± 17	$(1.52 \pm 0.11) \times 10^6$	0.65 ± 0.11	140 ± 16	167 ± 15	1388 ± 127
121 ± 19	$(3.22 \pm 0.23) \times 10^4$	–	–	73 ± 8	1003 ± 94
306 ± 30	$(1.06 \pm 0.08) \times 10^6$	0.04 ± 0.01	22 ± 5	33 ± 3	827 ± 76

librium, due to the mass difference, the relative velocity between the e^+ 's and the \bar{p} 's is predominantly due to the positron plasma temperature.

The positron plasma was characterized by a typical length of 32 mm, radius of 2.5 mm, particle number 7×10^7 , number density $1.7 \times 10^8 \text{ cm}^{-3}$ and storage time of thousands of seconds. These quantities have been measured using a nondestructive plasma modes diagnostic method based on the observation of the first two axial modes of a finite temperature plasma [21,22]. The reproducibility of the results, over several weeks and under different conditions, was good. Maximum variations in density of about 30% were observed.

During mixing the positron plasma temperature could be changed in a controlled way by RF excitation of the axial dipole mode of the plasma. Heating was achieved by the application of a radio frequency drive to one of the electrodes with a 2 MHz span across the dipole mode resonance (typically around 20 MHz) at a sweeping frequency of 1 kHz. Excitation at the dipole mode ensures that the plasma reaches thermal equilibrium rapidly [17]. A measured shift in the quadrupole frequency was used to calculate the magnitude of the temperature change with a reasonable uncertainty [21,22]. The minimum measurable temperature increase was about 15 meV ($\simeq 175 \text{ K}$). Note that the modes diagnostic yields only relative temperature changes and not the absolute temperature of the positron plasma. The electrode temperature of 15 K is

thus the lower limit for the unheated plasma temperature, and we adopt this as our unperturbed temperature.

Mixing of positrons and antiprotons was carried out for different positron plasma temperatures (Table 1). Four samples contained enough data to allow a detailed analysis of antihydrogen production, as described in [1]. This set includes the so-called “cold mixing” where no heating was applied, as well as three samples with $\Delta T = 15 \pm 15 \text{ meV}$ ($\simeq 175 \text{ K}$), $\Delta T = 43 \pm 17 \text{ meV}$ ($\simeq 500 \text{ K}$) and $\Delta T = 306 \pm 30 \text{ meV}$ ($\simeq 3500 \text{ K}$, “hot mixing” sample).

For the two samples in Table 1 with a temperature increase lower than our resolution of 15 meV, a linear correlation between the applied heating voltage and the temperature increase was assumed. A quadratic behaviour, possible in this regime of low heating power, would result in very similar ΔT 's, the differences being well within the uncertainties associated to these temperatures.

2.3. Antihydrogen signal

For clarification it should be stressed that in the following antihydrogen production refers only to antiatoms that annihilate on the walls of the charged particle trap within the detector volume. The detector solid angle coverage for $\bar{\text{H}}$ emerging isotropically from the trap center and annihilating at the electrodes is estimated to be $\sim 98\%$ by Monte Carlo calculation.

Antihydrogen formation was previously [1] demonstrated by full reconstruction of the simultaneous annihilation of the \bar{p} and e^+ . After the determination of the position of the \bar{p} annihilation vertex, we search for clean evidence of e^+ annihilation 511 keV photons in the CsI crystal data. A charged particle track intercepting a crystal eliminates that crystal and its eight nearest neighbors from consideration. For each of the remaining crystals we require an energy deposit in the 511 keV window and no deposit in any of the adjacent ones. We select only those events which have a vertex and two crystals passing these criteria. The “opening angle” ($\theta_{\gamma\gamma}$) is the angle, as seen from the annihilation vertex, between these two crystals. An ideal \bar{H} event will have an opening angle of 180° , corresponding to $\cos(\theta_{\gamma\gamma}) = -1$. \bar{H} annihilations may also produce events with $\cos\theta_{\gamma\gamma} > -1$, since the 511 keV γ 's from the positron annihilation may be undetected and replaced by low energy γ 's. These background γ 's are generated in electromagnetic showers created by high energy γ 's coming from neutral pion decay. Such pairs of photons have no angular correlation with the antiproton vertex. This is confirmed by the opening angle distribution of a Monte Carlo simulation of pure \bar{H} annihilations (Fig. 1(a)).

The opening angle distributions for four different temperatures are shown in Fig. 1(b)–(e). All distributions except that for hot mixing show an excess of events at $\cos(\theta_{\gamma\gamma}) = -1$. The “opening angle excess”, defined as the number of events with $\cos(\theta_{\gamma\gamma}) \leq -0.95$ exceeding the central plateau (see Table 1), is shown as a function of the temperature in Fig. 3(a). This number is proportional to the total number of \bar{H} atoms produced during a standard cycle.

In order to further study \bar{H} formation at various positron temperatures we analyze our measurements in a variety of ways that may be used as proxies for the direct detection of the antihydrogen annihilation event. We have shown in a previous publication [11] that in cold mixing the antihydrogen annihilations account for a significant fraction ($\sim 65\%$) of the trigger rate. Fig. 2 shows the trigger rates in the first 3 s of mixing for the four samples with high statistics. In Table 1 the number of triggers in the time windows 0–3 s and 0–180 s, where 0 is the start of mixing and 180 s is the maximum mixing interval are reported. These values are corrected for the trigger

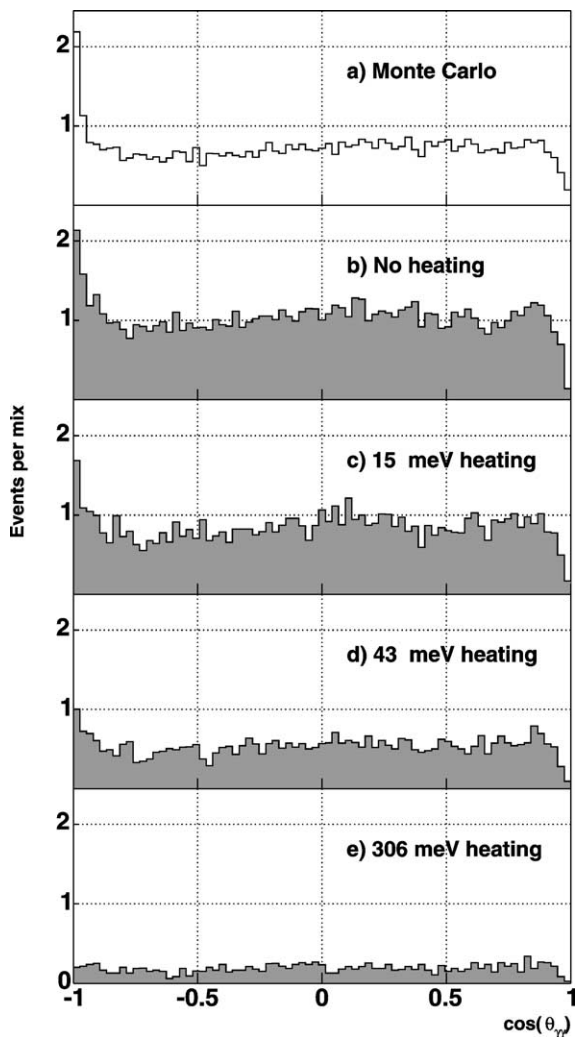


Fig. 1. Distribution of $\cos(\theta_{\gamma\gamma})$ for different positron plasma temperatures. (a) Monte Carlo simulation of a pure \bar{H} sample, (b)–(e) measured distributions for positron plasma temperatures with high statistics. The distributions were normalized to a standard mixing cycle with 10^4 \bar{p} 's.

efficiency. The total number of triggers during mixing as a function of the positron plasma temperature is shown, for all the samples, in Fig. 3(b). The hot mixing data were interpreted as the background due to \bar{p} -only annihilations and were subtracted from the other samples. The temperature dependence of the trigger data is very similar to that of the opening angle excess. This suggests that the integrated number of triggers, after hot mixing background subtraction, is

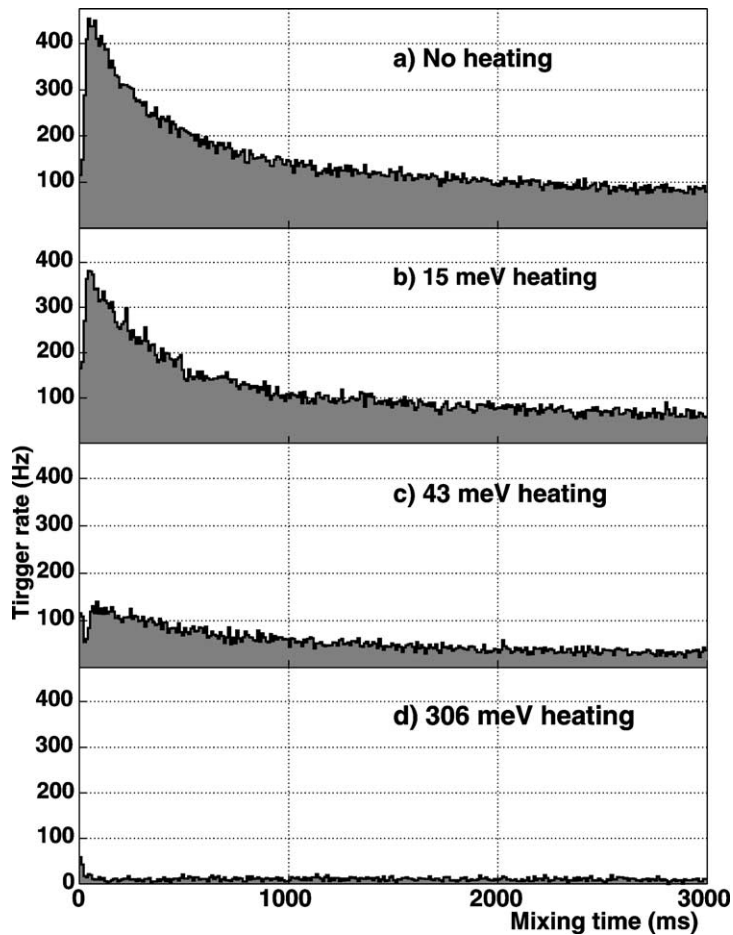


Fig. 2. Trigger rates in the first 3 seconds for 4 different positron plasma temperatures corresponding to high statistics samples. The complete samples have been scaled to a single standard mixing cycle with $10^4 \bar{p}$'s.

a good proxy for antihydrogen formation not only in cold mixing, as previously shown in [11], but also in the heated samples described here.

We have also looked at the “peak trigger rate” defined as the maximum value of the detector trigger rate after the start of mixing, excluding the first 20 ms when some \bar{p} 's can be lost immediately upon the injection into the nested trap. Note that for the samples where antihydrogen production (Fig. 2) is present a dramatic increase in the rate of annihilations is observed when antiprotons are injected into the positron plasma. A more detailed discussion of the antihydrogen formation time dependence is beyond the scope of this Letter, but we note that the decay of

the trigger signal in time is not due only to depletion of the antiproton sample due to \bar{H} production. Spatial decoupling of the two particle clouds also plays a role. The peak trigger rate as a function of the plasma temperature is shown in Fig. 3(c) and the values, corrected for the trigger efficiency, are reported in Table 1. We have previously shown [11] that integrated over the first second of mixing, more than 85% of the triggers are due to \bar{H} production. We expect this percentage to be even higher for the peak trigger rate. If we use the hot mixing as a background (see Table 1) we can estimate this fraction to be around 95%, corresponding to an absolute instantaneous \bar{H} rate of 432 ± 44 Hz.

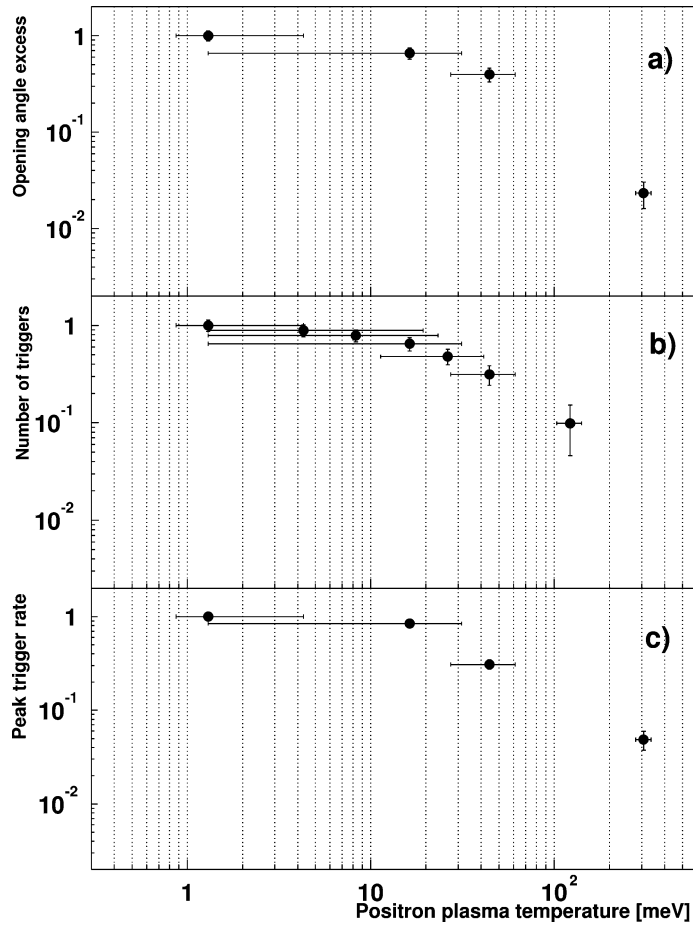


Fig. 3. Temperature dependence of $\bar{\text{H}}$ production using different variables. All the quantities are normalized to the cold mixing sample. They are displayed as a function of the absolute positron plasma temperature assuming a cold mixing temperature of 15 K. (a) Opening angle excess for the high statistics samples, (b) number of triggers for all the samples (the *hot mixing* sample has been used as background, thus it is not shown), (c) peak trigger rate for the high statistics samples.

3. Discussion

As indicated earlier, two processes have traditionally been expected to be relevant for formation of $\bar{\text{H}}$ during mixing of \bar{p} 's and e^+ 's. In the radiative process, a photon carries away the excess momentum and energy, and the formed atoms are strongly bound with typical principal quantum numbers $n < 10$ ($E_b > 136$ meV). In zero magnetic field the rate for this process is expected to scale approximately as $T^{-0.63}$ [7]. In the three-body process, an additional positron carries away excess momentum and energy. Formation by this mechanism leads initially to weakly bound states with $E_b \sim k_B T$ (1.3 meV at 15 K),

that are easily ionized by collisions in the positron plasma. Some of these atoms will collisionally de-excite and become more tightly bound. The expected temperature dependence in an infinite positron plasma is $T^{-9/2}$ for formation of states that are resilient to re-ionization [23]. The threshold, also called the “bottle-neck”, below which atoms will survive collisional ionization is $E_b^{\text{th}} \sim 4k_B T$ (5.2 meV at 15 K) [23].

We must first note that the three curves in Fig. 3 contain slightly different information. The opening angle excess is a definitive measurement of the total integrated antihydrogen production for the 180 s mixing cycle. The same is true of the total number of triggers after background subtraction. Both of

these integrated plots are sensitive to effects such as spatial decoupling of the two particle clouds, and in that sense cannot be used as indications of instantaneous combination rate. The peak trigger rate is thus a “cleaner” measurement of the combination rate, reflecting the conditions of best overlap at the time when we believe that the antiprotons are closest to thermal equilibrium with the positrons.

We thus examine the peak trigger rates in Fig. 3(c) for compatibility with the predictions for the two production mechanisms. Several general features are evident. First, the antihydrogen production is observed to decrease with increased positron plasma temperature, as expected. (This effect was used in previous work to suppress the antihydrogen formation [1].) It is interesting to note that antihydrogen is clearly present for room temperature positrons. The second main feature is that the formation does not scale as a simple power law with the positron temperature. There is a clear turnover of the rate at low temperature. Furthermore, all attempts to fit the data with combinations of power laws, e.g., representing a mixture of two- and three-body processes, are unsuccessful. The presence of the latter is expected to be most pronounced at temperatures below ~ 10 meV ($\simeq 100$ K) [24]; the lower temperature data are however characterized by a leveling-off, rather than an increase. The naive scaling for the three-body reaction, $T^{-9/2}$, is clearly inconsistent with our data. It should be noted that collisional relaxation and finite transit time of the antiprotons through the positron plasma can lead to a different temperature scaling for the three-body reaction [7,25,26].

We have also considered whether the radiative reaction is the dominant process. The agreement of this model is reasonable, at least as far as the scaling with temperature is concerned. Even though a simple power law is not able to fully reproduce the behaviour of our data a best-fit power law to the peak trigger rate curve (Fig. 3(c)) yields a dependence of $T^{-0.7\pm 0.2}$ (compared to $T^{-0.63}$ in [7]). We next consider a simple estimate of the absolute magnitude for the radiative process. Using the radiative combination cross section σ_{rad} given in [5,27], summed over all the Rydberg states able to survive the field ionization and assuming a Maxwellian distribution for the positron plasma the radiative combination rate R_{rad} can be expressed as [24]

$$R_{\text{rad}} = N_{\bar{p}} n_{e^+} \left[\frac{m}{2\pi k_B T} \right]^{3/2} \times \int v \sigma_{\text{rad}}(v) e^{-mv^2/2k_B T} d^3v, \quad (1)$$

where m is the reduced mass, v is the modulus of the relative velocity between \bar{p} 's and e^+ 's, $N_{\bar{p}}$ the total number of \bar{p} , n_{e^+} the positron plasma density and $d^3v = 4\pi v^2 dv$ in the case of pure isotropy. Following our simple assumptions, the peak trigger rate should be comparable to R_{rad} . Given a temperature of 15 K, and assuming complete overlap between the two particle clouds, we calculated an antihydrogen production rate due to radiative combination in the ATHENA conditions of about 40 Hz for 10000 \bar{p} 's and $1.7 \times 10^8 \text{ cm}^{-3}$ positron plasma density. If we compare this value with our measured value of 432 ± 44 Hz we clearly see that the experimental result is one order of magnitude higher. In other words the absolute measured production rate is not obviously compatible with a simple radiative calculation. Note that any possible effects of the magnetic field are not taken into account in the simple calculation above.

The dynamics of the antihydrogen formation and transport to the walls is intricate. In addition to the processes mentioned above, radiative and three-body combination into well-defined quantum states, the particles in a strong magnetic field may also form weakly bound, “guiding center” atoms [23]. Any weakly-bound antihydrogen atoms formed may be ionized by collisions in the plasma or by the electric fields of the trap or the positron plasma itself. The atoms formed in an excited state will tend to decay towards the ground state and become stabilized against ionization. The detectable antihydrogen flux is thus determined by the competition of the formation/decay chain with the ionization processes.

For all of our detection schemes, the antihydrogen atoms must drift to the wall and annihilate there. The antiatoms must pass the combined fields of the positron plasma and the nested trap without being ionized. Roughly speaking, loosely bound atoms will be ionized by electric fields greater than $F = (E_b/0.38 \text{ meV})^2$ [28], where E_b is their binding energy in meV and F is expressed in V cm^{-1} . The peak electric field may be calculated from the positron plasma measurements and the known electrode configuration, and lies between 40 and 60 V cm^{-1} depending

on the drift direction of the antiatom. In our apparatus the escaping atoms must thus have $E_b > 2.4$ meV to be able to reach the wall.

The turnover in the production rate at low temperature is not yet understood. There is a minimum velocity scale associated with the positron plasma rotation, but this velocity is radius-dependent and even the maximum (about 10^4 m s⁻¹) is too small to explain the position of the observed turnover. This turnover may be associated with the complex equilibrium between formation and ionization processes, although experimental uncertainty in the measured temperature change may also be important.

4. Conclusions

Summarizing, the temperature dependence of the antihydrogen production has been studied for the first time. A clear decrease of the antihydrogen production with the positron plasma temperature has been seen, but a simple power law scaling does not fit the data. The naive three-body temperature dependence ($T^{-9/2}$) is not consistent with our data and the expected predominance of this mechanism below ~ 100 K is not supported by the leveling-off at low temperatures. The fall-off in antihydrogen production is slow enough that it is still measurable at room temperature in the ATHENA apparatus. This observation, coupled with the behavior at high temperature, suggests that the radiative mechanism cannot be completely excluded in ATHENA, leading to antiatomic states that are more tightly bound than those observable using field ionization techniques. Nevertheless the radiative \bar{H} production rate prediction is not obviously compatible with our measurement, the former being an order of magnitude lower.

Theoretical guidance is necessary for further progress in understanding the complex interplay of production and ionization processes in ATHENA. The effect of the magnetic field, the polarization of the positron plasma by the injected antiprotons, and the role of guiding center atoms need to be considered in detail in order to fill in the picture. Simulation of the dynamics of antiproton slowing and combination processes is certainly needed for the conditions of our experiment. Simulations are in progress that suggest that the finite transit time of the antiprotons through

the positron plasma plays an important role for three body processes [26]. The experimental challenges that emerge from our study include precise determination of the positron temperature and density, determination of the spatial overlap of the positron and antiproton clouds, and analysis of the detailed time-dependent dynamics of the positron–antiproton interaction. The current inability to diagnose tightly bound states is also a barrier to understanding, highlighting the desirability of studying laser interactions with antiatoms at the earliest possible time.

The unique positron plasma diagnostics and control developed for ATHENA have made measurements of antihydrogen production as a function of positron plasma temperature possible. The detection mechanism employed in ATHENA also offers a first look into the dynamical time development of the combination process. The promise of understanding and, perhaps more importantly, controlling this complex process with a view towards trapping of neutral antihydrogen is now within experimental reach.

Acknowledgements

This work was supported by the following agencies: Istituto Nazionale di Fisica Nucleare (Italy), Conselho Nacional de Pesquisa e Desenvolvimento (CNPq), Fundacao de Amparo a Pesquisa do Estado do Rio de Janeiro (FAPERJ) e Fundacao CCMN/UFRJ (Brazil), Grant-in-Aid for Creative Basic Research of Monbukagakusho (Japan), the Swiss National Science Foundation, the Danish Natural Science Research Council, the UK Engineering and Physical Sciences Research Council.

References

- [1] M. Amoretti, et al., *Nature* 419 (2002) 456.
- [2] G. Gabrielse, et al., *Phys. Rev. Lett.* 89 (2002) 213401.
- [3] G. Gabrielse, et al., *Phys. Lett. A* 129 (1988) 38.
- [4] M.H. Holzscheiter, M. Charlton, *Rep. Prog. Phys.* 62 (1999) 1.
- [5] H.A. Bethe, E.E. Salpeter, *Quantum Mechanics of One- and Two-Electron Systems*, Springer, Berlin, 1957.
- [6] P. Mansback, J.C. Keck, *Phys. Rev.* 181 (1969) 275.
- [7] J. Stevefelt, J. Boulmer, J.-F. Delpech, *Phys. Rev. A* 12 (1975) 1246.
- [8] M. Niering, et al., *Phys. Rev. Lett.* 84 (2000) 5496.
- [9] C.L. Cesar, et al., *Phys. Rev. Lett.* 77 (1996) 255.

- [10] T.M. O’Neil, Phys. Fluids 23 (1980) 725.
- [11] M. Amoretti, et al., Phys. Lett. B 578 (2004) 23.
- [12] C. Regenfus, Nucl. Instrum. Methods A 501 (2003) 65.
- [13] M. Amoretti, et al., CERN-EP/2003-051, Nucl. Instrum. Methods A 518 (2004) 679.
- [14] L.R. Brewer, et al., Phys. Rev. A 38 (1988) 859.
- [15] T.M. O’Neil, C.F. Driscoll, Phys. Fluids 22 (1979) 266.
- [16] C.F. Driscoll, J.H. Malmberg, K.S. Fine, Phys. Rev. Lett. 60 (1988) 1290.
- [17] B.R. Beck, J. Fajans, J.H. Malmberg, Phys. Plasmas 3 (1996) 1250.
- [18] G. Gabrielse, et al., Phys. Lett. B 507 (2001) 1.
- [19] Y. Chang, C.A. Ordonez, Phys. Rev. E 62 (2000) 8564.
- [20] C.A. Ordonez, et al., Phys. Plasmas 9 (2002) 3289.
- [21] M. Amoretti, et al., Phys. Rev. Lett. 91 (2003) 055001.
- [22] M. Amoretti, et al., Phys. Plasmas 10 (2003) 3056.
- [23] M.E. Glinsky, T.M. O’Neil, Phys. Fluids B 3 (1991) 1279.
- [24] A. Müller, A. Wolf, Hyperfine Interact. 109 (1997) 233.
- [25] P.O. Fedichev, Phys. Lett. A 226 (1997) 289.
- [26] F. Robicheaux, private communication.
- [27] L.H. Andersen, J. Bolko, Phys. Rev. A 42 (1990) 1184.
- [28] C.F. Driscoll, comment on “Driven Production of Cold Antihydrogen and the First Measured Distribution of the Antihydrogen States”, Phys. Rev. Lett., submitted for publication.